Journal of Fluids and Structures (1999) **13,** 681–708
Article No.: jfls. 1999.0228, available online at http://www.idealibrary.com on IDEAL

THE FLUID–STRUCTURE INTERACTION IN SUPPORTING A THIN FLEXIBLE CYLINDRICAL WEB WITH AN AIR CUSHION

S. MÜFTÜ

Massachusetts Institute of Technology, Haystack Observatory, Westford, MA 01886, U.S.A.

AND

K. A. COLE

Eastman Kodak Company, Rochester, NY 14652, *U.S.A.*

(Received 6 October 1998 and in revised form 25 March 1999)

The mechanics of the fluid–structure interaction between a thin flexible web, wrapped around a cylindrical drum (reverser), and the air cushion formed by external pressurization through the holes of this drum is analyzed. Derivation of a "new" theory for the moderately large deflections of a thin cylindrical shell to model the web is presented. This theory allows for large web deflections, while using a self-adjusting strain-free reference state for the web in order to keep the circumferential web tension around a constant level. The theory also incorporates the redistribution of the in-plane stress resultants in the axial and shear directions using the Airy stress function. The air-flow is averaged over the height direction of the web-reverser clearance. The surface area of the pressure holes is averaged locally over the total reverser surface. The resulting equations are a modified form of the Navier–Stokes and mass balance equations with nonlinear source terms. The coupled fluid–structure system is solved numerically. The mechanics of the interaction between the web deflections and the air cushion generated by the reverser is explained. The effects of the problem parameters on the overall equilibrium are presented. Parameter distributions which cause the web to contact the reverser are identified, and suggestions are made to avoid this state. © 1999 Academic Press

1. INTRODUCTION

1.1. DESCRIPTION OF THE PROBLEM

AN AIR-REVERSER IS A HOLLOW, cylindrical, porous drum used in web-handling applications where it is important to change the direction of a web without contact. An air cushion is formed in the web-reverser clearance by injecting pressurized air through the holes of the reverser. The web floats over this air cushion and the direction of the moving web is thus changed without contacting the underlying drum. A schematic depiction of a web floating over a reverser is given in Figure 1. The magnitude of the overall floating pressure p_{ave} depends primarily on the pull-down pressure T/R due to wrapping the web under tension T over a drum with radius R. A typical web path is equipped with an active tension control mechanism that keeps the web tension constant. Therefore, relatively large web deflections can be implemented without inducing large strains.

0889–9746/99/060681 + 28 $30.00 © 1999 Academic Press

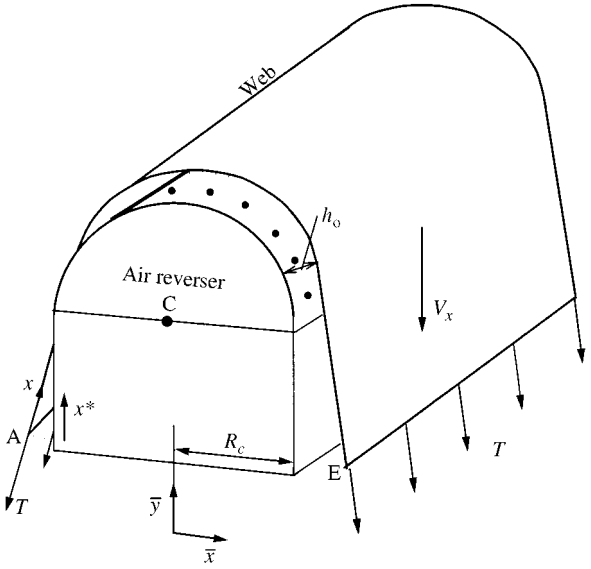

Figure 1. Schematic view of a web moving over an air reverser under tension T and with speed V.

The steady-state air pressure in the interface is inversely related to the web- reverser clearance h (Müftü *et al.* 1998a). Therefore, while the air injected into the clearance causes the web to deflect away from its initial state, increasing clearance causes reduction in the air pressure. Thus the fluid mechanics of air is coupled to the deflection of the web and *vice versa*. The coupled system eventually settles to a steady-state clearance.

1.2. The Fluid Mechanics of an Air Reverser

Typical web-reverser clearance (3–4 mm) is considerably smaller than the typical width (1 m) and length (1 m) of the web supported by the reverser. The air-flow in this narrow clearance is primarily dominated by inertial flow (Müftü *et al.* 1998a). The viscous flow contribution constitutes a relatively small (10–20%) fraction of the average air pressure in the clearance (Müftü *et al.* 1998b). The velocity of the moving web is typically 2–5 m/s, whereas the velocity of air in the web-reverser clearance is typically 20 m/s. The effect of the web velocity on the air pressure is therefore neglected in this work. The stronger inertial flow effect can be seen when the ratio of inertial to viscous forces in the fluid, given by the modified Reynolds number $\mathrm{Re}^* = \rho V h^2/\mu L$, is calculated. For the typical clearance height $h = 4$ mm, wrap-length $L = 1$ m, flow speed $V = 20$ m/s, air density $\rho = 1{\cdot}2$ kg/m^3 and air viscosity $\mu = 1{\cdot}85 \times 10^{-5}$ Pa s, the modified Reynolds number is 21. The two-dimensional air-reverser flow model presented by Müftü *et al.* (1998a, b) use the fluid velocities u^* and v^*, in the plane of the web, and the air pressure p averaged over the web-reverser clearance. The fluid velocity w^* in the clearance-height direction is neglected. The governing equations of the flow are a modified form of the incompressible Navier-Stokes and mass balance equations with nonlinear source terms.

A problem similar to the fluid–structure interaction of a web and a reverser is encountered in externally pressurized foil bearings (Gross 1980). However, a close look at typical parameters of a foil-bearing application: tape-guide clearance $h = 2$ μm, wrap-length $L = 5$ mm and tape speed 2 m/s, shows that the modified Reynolds number is 10^{-4}. This

indicates that viscous forces strongly dominate the flow. Moreover, the air-entrainment effects on the downstream side of the groove region also play a dominant role in the pressure developed in the interface (Wildmann 1969; Eshel 1979). The fluid mechanical effects in the foil bearing problem seem to be substantially different from that in the air-reverser problem.

The interaction of a single Coanda jet with a flexible flat web has been studied by Quadracci & Modi (1994), where the web is assumed to be infinitely wide. The main fluid mechanical effect in this case is the creation of a reliable source of air-suction to stabilize the web. An experimental study on this subject has been reported by Pimenov & Galimov (1994).

1.3. Mechanics of a Thin Flexible Web Wrapped around a Cylinder

In this paper, web deflections are modeled by a moderately large deflection "cylindrical" shell theory with a continuous curvature variation and a *self-adjusting reference state*, near the steady state of the web. This new approach creates an efficient method in representing the deflection history of the web, arising from its initial wrapping around the drum and its subsequent motions to keep a nearly constant tension level.

The shell theory used here is based on an extension of Donnell's (1976) theory on cylindrical shells. Donnell's work is an extension of von Karman's plate theory, which has been used by Lin & Mote (1995, 1996) to study the buckling of a flat web in the free span between two rollers. The subject of wrapping a thin web around a cylindrical drum, over large wrap-angles was treated by Rongen (1990, 1994) who used Donnell's theory. Sundaram & Benson (1989) and Müftü & Benson (1995) used the small-deflection cylindrical shell theory to study the dynamic effects in this problem. Ono & Ebihara (1984) also used the cylindrical shell equations in obtaining steady-state solutions related to tape mechanics. In these works, neither the web curvature containing a discontinuity at the tangency point, which can only be correct for vanishingly thin membranes, nor the "straight" region of the web are considered. In the present work, a continuous function for the curvature variation of a relatively thick web, wrapped around a cylindrical drum, is introduced. The continuous web curvature, as it will be defined here, has also been treated recently by Benson (1998).

A self-adjusting reference state in connection with the analysis of flexible tapes was first described by Barlow (1967). The in-plane stresses were referred to a self-adjusting cylindrical surface as described here, but the bending moments were described with respect to the undeflected configuration w_0, in contrast to the present work. The equations were, then, reduced to an infinitely wide web where the effects vanish. Benson & D'Errico (1991) and Benson (1993) used an adjustable reference radius in their work, where they considered the radial deflections of a cylindrical shell wrapped around a bumpy drum. They considered only the circumferentially symmetrical case. In their model an initially unknown *reference radius* is defined where the in-plane stresses vanish. A constraint equation, based on averaging the radial deflections and on keeping the circumferential in-plane stress resultant at the level of the externally applied tension, is used to find this reference radius.

Description of the present shell model

Consider an initially flat web L_x long and L_y wide, simply supported at its longitudinal ends and free on its lateral edges. This web is first wrapped around a cylindrical drum, and then it is further deflected by air pressure. During this process, the longitudinal tension in the web

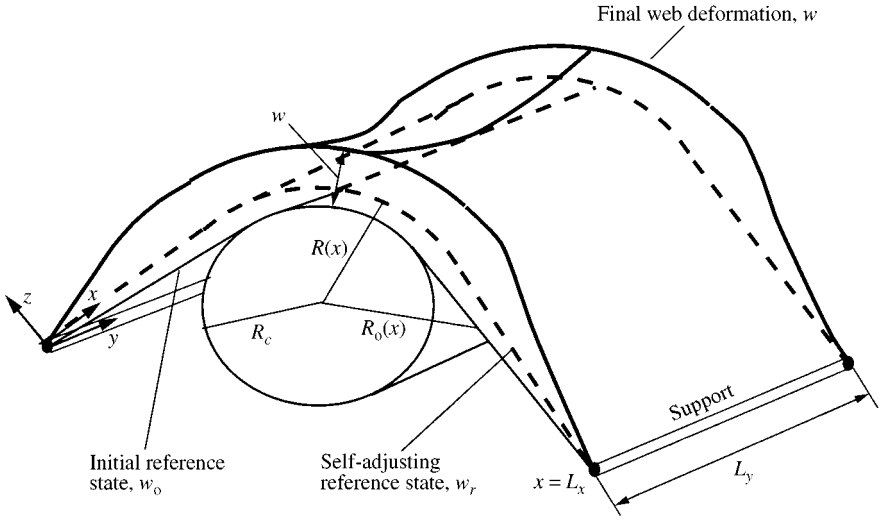

Figure 2. Schematic depiction of the strain-free reference w_r and the total deflection w for a web wrapped around a cylinder of radius R_c.

remains constant, while the length of the web between its supports changes. This is a fairly complicated deflection history which can be analyzed by nonlinear continuum mechanics [e.g., Bathe (1996)].

A different approach is taken in this paper, where partial differential equations of moderately large-deflection shell theory are derived, based on the final deflected state of the web. The deflection history of the web is directly included in these equations, based on the knowledge of the various states of this deflection. Therefore, this approach can best be described by referring to these different states. There are two key configurations used in this model: the *initial*, w_0, and the *self-adjusting*, w_r, reference states. The actual, final configuration of the web is indicated by w. These states are schematically depicted in Figure 2.

When a quiescent web is wrapped around a cylindrical drum, it comes in contact with the drum in the *wrap-region* and its curvature off the drum asymptotically approaches zero. This is called the *initial reference state*, w_0. The deflection history of bending the web around the drum is included in this state.

When the web finds its actual, steady-state configuration w due to fluid–structure coupling, its length will increase with respect to w_0, but its tension will remain the same. Thus, despite the large deflections that the web undergoes, it is strained only moderately. Therefore, the strain-free state of the web can no longer be the initial reference state. It would be reasonable to assume, since the web tension remains constant, that the strain-free state of the web moves with the web. Thus the self-adjusting reference state, w_r, from which the web strains are measured, is described by a "cylindrical" surface extending from the mid-line of the deflected web in the lateral direction. In mathematical notation the self-adjusting reference state is indicated by

$$w_r(x) = w(x, \tfrac{1}{2} L_y). \tag{1}$$

The self-adjusting reference state varies only along the running direction x. This is necessary, in order to be able to use the cylindrical shell theory to represent the web deflections. The variability of the web curvature in the x-direction does not represent a problem, as long as the local web curvature does not deviate too much from the state defined by w_0 (Donnell

1976; p. 360). The self-adjusting reference state w_r is initially unknown and its shape strongly depends on the air pressure acting on the web.

The web deflection which causes the local straining occurs with respect to the self-adjusting reference state w_r. This deflection is defined as

$$\bar{w} = w - w_r. \tag{2}$$

The moderately large-deflection shell theory used in this work allows the deflection $\bar{w}$ of a typical web to be in the order of the web thickness, i.e., 0·1–0·2 mm (Donnell 1976; p. 360).

Bending the web around a cylindrical drum causes anticlastic curvature $\nu/R(x)$ to develop in the transverse direction of the web, where ν is the Poisson ratio (Timoshenko & Woinkowsky-Krieger 1987). Fung & Wittrick (1955) indicate that the web cross- section remains mostly flat in the transverse direction if the ratio $(L_y/2)^2/(Rc)$ is large. An exception to this occurs in the deflection boundary layers around the lateral edges, where the maximum web deflection is still less than the web thickness. For a typical web thickness $c = 0{\cdot}2$ mm, drum-radius of 0·25 m and web width of 1 m this ratio is approximately 5000; thus the effect of the anticlastic curvature is neglected in this work.

2. WEB DEFLECTION EQUATIONS

The derivation of the equations governing the web deflections given in the following are based on the theory of cylindrical shells by Donnell (1976). In the present work, the in-plane strains and the curvatures of the web are measured from an initially unknown, *self-adjusting reference state*, w_r; The radius of curvature of the web $R(x)$ is a continuous function of the circumferential direction x. In this work, the coordinate axes are oriented in such a way that the positive pressure p and radial deflection w are oriented along an outward normal to the shell surface. The circumferential direction is denoted by x and the transverse direction by y.

The classical shell theory is based on the Kirchoff–Love assumptions which state that: (i) the thickness of the shell is small compared to the other dimensions of the shell; (ii) normals to the undeflected middle surface of the shell remain straight and normal to the deflected middle surface; (iii) the transverse normal stress σ_z can be neglected compared to other stresses; (iv) the deflections of the shell $\bar{w}$ are small compared to the thickness of the shell, c (Donnell 1976). This last assumption leads to the small-deflection shell theory where the deflection is mainly dominated by bending of the shell and the middle-surface stretching is only due to external tension applied at the edges.

For larger web deflections that are in the order of the web thickness, bending of the shell contributes significantly to its in-plane stretching. In this case, the in-plane and bending equilibria of the shell are coupled, and the membrane strains become nonlinear (Donnell 1976):

$$\varepsilon_x = \frac{\partial u}{\partial x} + \frac{\bar{w}}{R(x)} + \frac{1}{2}\left(\frac{\partial \bar{w}}{\partial x}\right)^2, \quad \varepsilon_y = \frac{\partial v}{\partial y} + \frac{1}{2}\left(\frac{\partial \bar{w}}{\partial y}\right)^2, \quad \varepsilon_{xy} = \frac{\partial v}{\partial x} + \frac{\partial u}{\partial y} + \frac{\partial \bar{w}}{\partial x}\frac{\partial \bar{w}}{\partial y}, \tag{3}$$

where u and v are the in-plane web deflections in the x- and y-direction, respectively. The nonlinear terms such as $(\partial\bar{w}/\partial x)^2$ represent the contribution of bending to the in-plane stretching of the web. The curvature of the shell after deflection is also measured with respect to the *self-adjusting reference state* and it is given by

$$\kappa_x = \frac{\partial^2 \bar{w}}{\partial x^2}, \quad \kappa_y = \frac{\partial^2 \bar{w}}{\partial y^2}, \quad \kappa_{xy} = \frac{\partial^2 \bar{w}}{\partial x \partial y}. \tag{4}$$

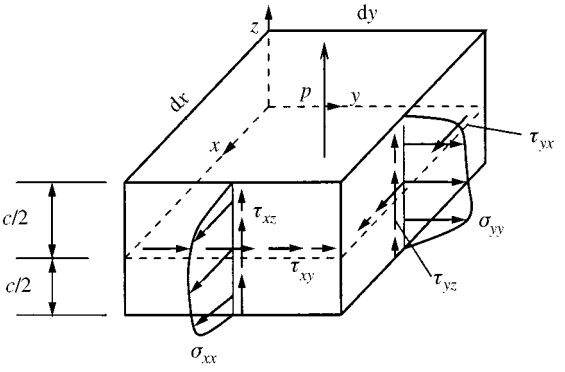

Figure 3. Stresses acting on a small rectangular piece of the web.

The equilibrium of the shell is expressed in terms of the stress resultants acting on the middle surface of the shell. These resultants are obtained by integrating the stresses through the thickness of the web, as depicted in Figure 3. Thus, the in-plane normal stress resultants N_x, N_y and the in-plane shear stress resultants N_{xy} are defined as

$$N_x = \int_{-c/2}^{c/2} \sigma_x \, \mathrm{d}z, \quad N_y = \int_{-c/2}^{c/2} \sigma_y \, \mathrm{d}z, \quad N_{xy} = \int_{-c/2}^{c/2} \tau_{xy} \, \mathrm{d}z, \tag{5}$$

where z is the coordinate axis perpendicular to the middle surface of the shell, τ_{xy} is the shear stress acting in the plane of the web, and σ_x and σ_y are the normal stresses acting in the circumferential and axial directions, respectively. The normal shear stress resultants Q_x and Q_y are defined as

$$Q_x = \int_{-c/2}^{c/2} \tau_{xz} \, \mathrm{d}z, \quad Q_y = \int_{-c/2}^{c/2} \tau_{yz} \, \mathrm{d}z, \tag{6}$$

where τ_{xz} and τ_{yz} are the shear stresses acting perpendicular to the plane of the web. The resultant moments M_x, M_y, and M_{xy} are defined as

$$M_x = \int_{-c/2}^{c/2} \sigma_x z \, \mathrm{d}z, \quad M_y = \int_{-c/2}^{c/2} \sigma_y z \, \mathrm{d}z, \quad M_{xy} = \int_{-c/2}^{c/2} \tau_{xy} z \, \mathrm{d}z. \tag{7}$$

Note that in shell theory it is generally assumed that $N_{xy} = N_{yx}$ and $M_{xy} = M_{yx}$ (Donnell 1976).

The equations governing the web deflections can be obtained by considering the equilibrium of the stress resultants acting on a small element of web, as shown in Figure 4 (Donnell 1976; Timoshenko & Woinkowsky-Krieger 1987). The in-plane components of the tractions acting on the web are indicated by f_x and f_y, and the normal component is indicated by p. In order to take the projections of the stress resultants on the coordinate axes x, y and z, an expression for the angle that the deformed surface makes with respect to the undeflected surface is needed. For moderately large deflections of the shell, this angle can be approximated by the slope of the deflected surface. For example, the slope of point A in Figure 4 is approximated by $\tan \theta_A \simeq \theta_A \simeq \partial w/\partial x$ and the slope of point B by $\tan \theta_B \simeq \theta_B \simeq \partial w/\partial x + \partial^2 w/\partial x^2$. Then, by taking the aforementioned projections, the following equilibrium equations are obtained:

$$\frac{\partial N_x}{\partial x} + \frac{\partial N_{yx}}{\partial y} = 0, \tag{8a}$$

$$\frac{\partial N_y}{\partial y} + \frac{\partial N_{xy}}{\partial x} = 0, \tag{8b}$$

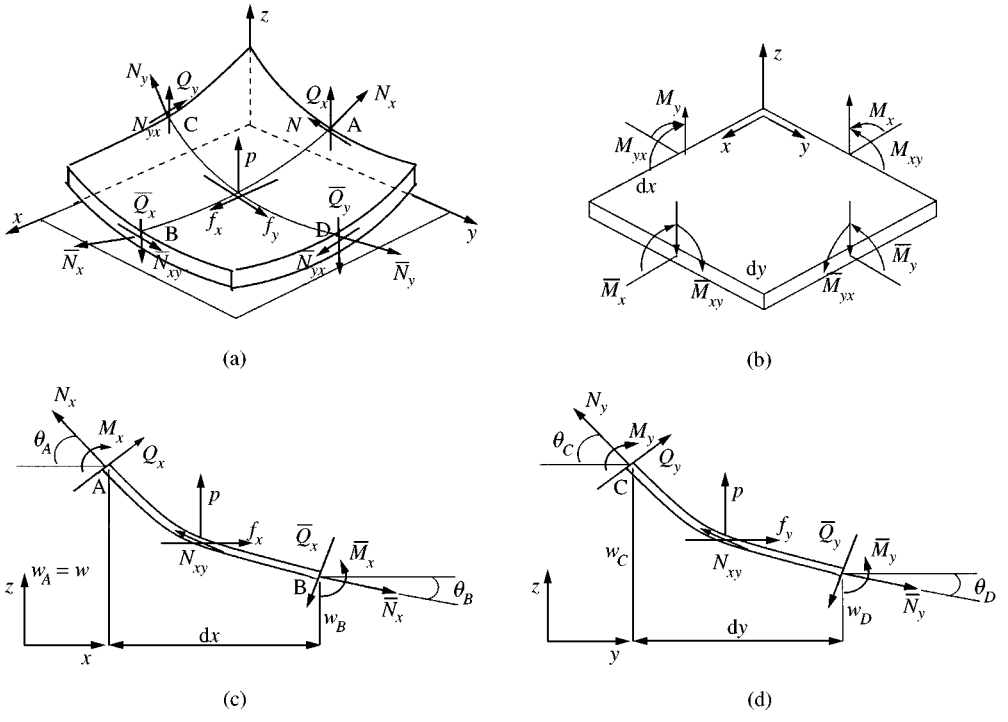

Figure 4. The stress and bending moment resultants acting on a piece of the web to keep the web in static equilibrium. Note that in this figure the bar over a variable indicates that it is incremented in the x-direction; such as $\bar{N}_x = N_x + (\partial N/\partial x)\,\mathrm{d}x$.

$$p - \frac{\partial Q_x}{\partial x} - \frac{\partial Q_y}{\partial y} + N_x\left(\frac{\partial^2 w}{\partial x^2} - \frac{1}{R(x)}\right) + N_y\frac{\partial^2 w}{\partial y^2} + 2N_{xy}\frac{\partial^2 w}{\partial x \partial y}$$

$$+ \left(\frac{\partial N_x}{\partial x} + \frac{\partial N_{yx}}{\partial y}\right)\frac{\partial w}{\partial x} + \left(\frac{\partial N_y}{\partial y} + \frac{\partial N_{xy}}{\partial x}\right)\frac{\partial w}{\partial y} = 0, \tag{8c}$$

where equations (8a) and (8b) are the in-plane equilibrium equations in x- and y-direction, respectively, and equation (8c) is the equilibrium equation in the z-direction.

The shell theory allows some simplification of the stress resultants in the derivation of equations (8a–c) (Donnell 1976, p. 173; Timoshenko & Woinkowsky-Krieger 1987, p. 379). First, the effect of the shear force resultants Q_x and Q_y, which are normal to the web surface, are neglected from the in-plane equilibrium equations (8a, b). As the local rotations of the web are small, the projection of Q_x and Q_y, on the in-plane directions would be negligible compared to the projections of N_x, N_y and N_{xy}. If included, these terms are $+\,Q_x(\partial^2 w/\partial x^2 - 1/R(x)) + \partial Q_x/\partial x\,\partial w/\partial x$ for equation (8a) and $+\,Q_y\,(\partial^2 w/\partial y^2) + \partial Q_y/\partial y\,\partial w/\partial y$ for equation (8b) on the left-hand side of these equations. Second, in deriving equation (8c) the variations of the in-plane stress resultants, such as $\partial N_{xy}/\partial x$, are neglected, as this variation is assumed to be small, compared to the stress resultant N_{xy}. Finally, the effect of the shear component of the external tractions f_x and f_y on the in-plane equilibrium equations are neglected, as this work does not consider the shear coupling between air and the web.

By considering the equilibrium of moments acting around the x- and y-axis, as shown in Figure 4(b), the moment equilibrium equations are obtained as

$$\frac{\partial M_y}{\partial y} + \frac{\partial M_{xy}}{\partial x} - Q_y = 0, \tag{9a}$$

$$-\frac{\partial M_x}{\partial x} + \frac{\partial M_{yx}}{\partial y} + Q_x = 0. \tag{9b}$$

The equation of equilibrium in the radial direction, equation (8c), can be further simplified by: (a) eliminating the last two terms of equation (8c) by using equations (8a, b) and (b) eliminating the normal shear force components Q_x and Q_y by using the moment equilibrium given by equations (9a, b). Then the following equation is obtained:

$$p + \frac{\partial^2 M_x}{\partial x^2} + 2\frac{\partial^2 M_{xy}}{\partial x \partial y} + \frac{\partial^2 M_y}{\partial y^2} + N_x\left(\frac{\partial^2 w}{\partial x^2} - \frac{1}{R(x)}\right) + N_y\frac{\partial^2 w}{\partial y^2} + 2N_{xy}\frac{\partial^2 w}{\partial x \partial y} = 0. \tag{10}$$

As the shear coupling between air and the web is neglected, at steady state, the in-plane stress resultant distribution N_x equals the externally applied tension T. However, local stress variations will exist in the web due to local differences in web deflection. If these local stress variations are indicated by N'_x, N'_y and N'_{xy}, then the stress resultants at steady state become

$$N_x = T + N'_x, \quad N_y = N'_y, \quad N_{xy} = N'_{xy}. \tag{11}$$

Hooke's law establishes the stress–strain, and the moment–curvature relations as follows:

$$\begin{Bmatrix} N'_x \\ N'_y \\ N'_{xy} \\ M'_x \\ M'_y \\ M'_{xy} \end{Bmatrix} = \begin{bmatrix} C & \nu C & 0 & 0 & 0 & 0 \\ \nu C & C & 0 & 0 & 0 & 0 \\ 0 & 0 & C' & 0 & 0 & 0 \\ 0 & 0 & 0 & D & \nu D & 0 \\ 0 & 0 & 0 & \nu D & D & 0 \\ 0 & 0 & 0 & 0 & 0 & D' \end{bmatrix} \begin{Bmatrix} \varepsilon_x \\ \varepsilon_y \\ \varepsilon_{xy} \\ \kappa_x \\ \kappa_y \\ \kappa_{xy} \end{Bmatrix}, \tag{12}$$

where

$$C = \frac{Ec}{1-\nu^2}, \quad C' = \frac{Ec}{2(1+\nu)}, \quad D = \frac{Ec^3}{12(1-\nu^2)}, \quad D' = D(1-\nu). \tag{13}$$

The stress resultant in the circumferential direction N_x from equation (11) can be expressed by using the Hooke's law and the definition of the strains as

$$N_x = T + C\left[\frac{\partial u}{\partial x} + \frac{\bar{w}}{R(x)} + \frac{1}{2}\left(\frac{\partial \bar{w}}{\partial x}\right)^2 + \nu\left(\frac{\partial v}{\partial y} + \frac{1}{2}\left(\frac{\partial \bar{w}}{\partial y}\right)^2\right)\right]. \tag{14}$$

By using this expression in equation (10) and by using Hooke's law, the equation governing the radial web deflections is obtained as

$$D\nabla^4\bar{w} + D_s\bar{w} - T\frac{\partial^2 w}{\partial x^2} - N'_y\frac{\partial^2 w}{\partial y^2} - 2N'_{xy}\frac{\partial^2 w}{\partial x \partial y} = p - \frac{T}{R(x)}, \tag{15}$$

where $D_s = Ec/(R^2(x)(1-\nu^2))$ is the shell-stiffness. This is the equation governing the radial deflections of the web. Note that this equation is nonlinear due to the presence of $\bar{w}$. The linear version of this equation (i.e., when $\bar{w} \to w$) has been used for modeling small

deflections of magnetic tapes by Ono & Ebihara (1984), Sundaram & Benson (1989) and Müftü & Benson (1995). In order to reduce the number of nonlinear terms in equation (15), the terms involving $\bar{w}(\partial^2 w/\partial x^2)$, $(\partial\bar{w}/\partial x)^2$ and $(\partial\bar{w}/\partial y)^2$ have been omitted. While these terms are important in retaining the ability to model large deflections, based on the success of the linear models mentioned above, this omission should not affect the results as long as the deflections $\bar{w}$ are in the order of web thickness. These nonlinear terms should be included in future work.

In equation (15), the in-plane stress resultants N'_y and N'_{xy} are unknown. They can be determined by a simultaneous solution of the in-plane equilibrium equations (8a, b) with equation (15). Alternatively, a single equation representing the in-plane stress resultants can be obtained by the method described by Donnell (1976, p. 361). This approach is adopted here. The in-plane equilibrium equations (8a, b) are identically satisfied by using the following definitions given in terms of the Airy-stress function $\phi(x, y)$:

$$N'_x = \frac{\partial^2\phi}{\partial y^2}, \quad N'_y = \frac{\partial^2\phi}{\partial x^2}, \quad N'_{xy} = -\frac{\partial^2\phi}{\partial x\partial y}. \tag{16}$$

The strain compatibility equation

$$\frac{\partial^2\varepsilon_x}{\partial y^2} + \frac{\partial^2\varepsilon_y}{\partial x^2} - \frac{\partial^2\varepsilon_{xy}}{\partial x\partial y} = 0 \tag{17}$$

ensures the uniqueness of the strain distribution. By using the membrane strains given by equation (3) in the strain compatibility equation the following equation is obtained:

$$\nabla^4\phi = Ec\left[\left(\frac{\partial^2\bar{w}}{\partial x\partial y}\right)^2 - \frac{\partial^2\bar{w}}{\partial x^2}\frac{\partial^2\bar{w}}{\partial y^2} + \frac{1}{R(x)}\frac{\partial^2\bar{w}}{\partial y^2}\right]. \tag{18}$$

Equations (15), (16) and (18) describe the equilibrium of a web wrapped around a cylindrical drum.

2.1. The Boundary Conditions

On the simple supports, the deflection $\bar{w}$ and the bending moment M'_x of the web are zero. On the free edges, the bending moments M'_y and the equivalent normal shear force resultant $Q_y^{\text{eq}} = Q_y + \partial M'_{xy}/\partial x$ vanish (Timoshenko & Woinkosky-Krieger 1987). These boundary conditions are expressed as

$$M'_x = D\left[\frac{\partial^2\bar{w}}{\partial x^2} + \nu\frac{\partial^2\bar{w}}{\partial y^2}\right] = 0, \tag{19a}$$

$$\bar{w} = 0, \tag{19b}$$

at $x = 0$, L_x, and $0 \le y \le L_y$; and at $y = 0$, L_y, and $0 \le x \le L_x$:

$$M'_y = D\left[\frac{\partial^2\bar{w}}{\partial y^2} + \nu\frac{\partial^2\bar{w}}{\partial x^2}\right] = 0, \tag{20a}$$

$$Q_y^{\text{eq}} = D\left[\frac{\partial^3\bar{w}}{\partial y^3} + (2-\nu)\frac{\partial^3\bar{w}}{\partial x^2\partial y}\right] = 0. \tag{20b}$$

The boundary condition for the Airy stress function is $\phi = 0$ around the periphery of the web.

2.2. The Curvature of the Web

Let $R_o(x)$ denote the radius of curvature of a web at the initial reference state when it is wrapped around a cylindrical drum. If this web has no bending stiffness ($D = 0$), then its radius of curvature will have a discontinuity at its tangency points L_1 and L_2. This type of curvature is expressed as

$$R_o(x) = R_c[H(x - L_1) - H(x - L_2)] \quad \text{for } 0 \leq x \leq L_x, \text{ and } 0 < L_1 < L_2 < L_x, \tag{21}$$

where H is the Heaviside step function. On the other hand, a web with finite bending stiffness ($D \neq 0$) wrapped around the same drum will not be able bend down to these tangency points. In fact, the new tangency points will be offset from L_1 and L_2 by a *peel-off angle* θ^*, as depicted schematically in Figure 5(a). In the *wrap-region*, the bending moment M in the web is simply given as

$$M = \frac{D}{R_c} \tag{22}$$

by Timoshenko & Woinkowsky-Krieger (1987). Sufficiently far away from the cylinder, in the *flat-region*, $1/R_o(x) \to 0$. Between these two ends a *transition region* exists, where $R_o(x)$ changes from R_c to ∞ in a continuous manner.

The *initial reference state* of the web is defined by the radius of curvature $R_o(x)$, the locations of the tangency points L_1, L_2 and the peel of angle θ^*. When the web deflects away from the initial reference state, its initial radius $R_o(x)$ and its final radius $R(x)$ are separated along the direction normal to the web, by w_r. This separation is small relative to the magnitude of $R_o(x)$, and it is neglected in this paper. Therefore, in the governing equations (15) and (18), $R(x) = R_o(x)$ is used.

In the following two sections, the Euler–Bernoulli beam theory and the elastica theory are used to obtain an expression for $R_o(x)$. The results of these two approaches are compared at the end of the section. It will be seen that the beam formulation leads to an analytical expression, while the elastica formulation requires a numerical solution. For ease of implementation, the beam formulation has been used in the governing equations.

2.2.1. *The web curvature using the beam equation*

In this section the equations describing the shape of the web in the transition and the flat-regions are derived by using the beam theory. For the derivation, consider only the length of the web $(L_2 - R_c\theta^*) \leq x \leq L_x$. Assuming that this region of the web can be modeled as a beam, its deflection can be found by solving

$$\frac{d^4 w}{ds^4} - \lambda^2 \frac{d^2 w}{ds^2} = 0, \tag{23}$$

where s is the coordinate axis of this beam oriented along the asymptote of the web, as shown in Figure 5(a), and $\lambda = (T/D)^{1/2}$. A bending moment M^* acts on this beam at $s = -s^*$, to satisfy the continuity of the beam with the web, and causes the beam to be deflected by an amount w^*. By using equation (22) we see that $M = M^*$. Thus, the following

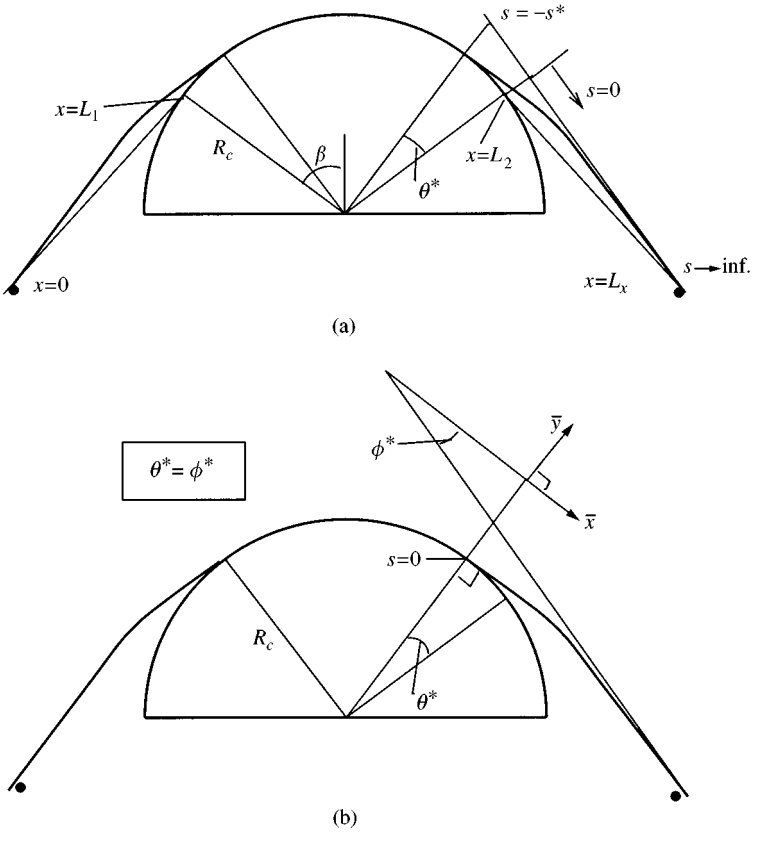

Figure 5. The schematic depiction of the *peel-off* effect due to web bending. (a) The coordinate system for the beam solution. (b) The coordinate system for the elastica solution.

boundary conditions describe the problem:

$$\text{at } s = -s^*: w = w^*, \quad \frac{d^2w}{ds^2} = \frac{1}{R_c}, \tag{24a,b}$$

$$\text{at } s \to \infty: w = 0, \quad \frac{dw}{ds} = 0. \tag{24c,d}$$

The solution of equation (23) with these boundary conditions gives

$$w = \frac{\exp[-\lambda(s^* + s)] - 1}{R_c\lambda^2} + w^*. \tag{25}$$

Note that the deflection w^* and the peel-off angle θ^* are not yet known. It can be shown that the slope of the beam at $s = -s^*$ is equal to the peel-off angle, i.e.,

$$\theta^* = \left.\frac{dw}{ds}\right|_{s=-s^*} = \frac{1}{R_c\lambda}. \tag{26}$$

An approximate equation for the variation of curvature along the web can then be found by assuming $\tan\theta^* \simeq \theta^*$ which leads to the relation $|s^*| \simeq R\theta^*$. The curvature variation thus

becomes

$$\frac{1}{R(s)} = \frac{\mathrm{d}^2 w}{\mathrm{d}s^2} = \frac{1}{R_c}\exp[-(1+\lambda s)]. \tag{27}$$

With this solution the curvature relation for the web wrapped around a cylindrical drum becomes

$$\frac{1}{R_o(x)} = \frac{1}{R_c}\begin{cases} \exp[-(1+\lambda(L_1 - x))], & 0 \le x \le L_1 + \dfrac{1}{\lambda}, \\ 1, & L_1 + \dfrac{1}{\lambda} \le x \le L_2 - \dfrac{1}{\lambda}, \\ \exp[-(1+\lambda(x - L_2))], & L_2 - \dfrac{1}{\lambda} \le x \le L_x. \end{cases} \tag{28}$$

2.2.2. *The web curvature using the equation of an elastica*

A more precise formulation of the web curvature variation can be obtained by using the inextensional elastica formulation (Frisch-Fay 1962; Benson 1998). The equation of moment equilibrium in this approach is given by

$$\frac{\mathrm{d}}{\mathrm{d}s}\left(D\frac{\mathrm{d}\psi}{\mathrm{d}s}\right) = -T\sin(\theta^* - \psi), \tag{29}$$

where s is the coordinate axis along the web whose origin is at the tangency point as shown in Figure 5(b), ψ is the angle between the tangent of the web at s and the $\bar{x}$ axis and θ^* is the orientation of the asymptote of the web. As stated before, θ^* is equal to the peel-off angle. Note that definitions of the coordinates s are different in Figures 5(a) and 5(b). The following relation exists between s and ψ:

$$s = \int_0^s \mathrm{d}\bar{s} = \frac{1}{\sqrt{2}\lambda}\int_0^\psi \frac{\mathrm{d}\bar{\psi}}{[1-\cos(\theta^* - \bar{\psi})]^{1/2}} \quad \text{for } \psi \in [0, \theta^*]. \tag{30}$$

The boundary conditions to solve equation (29), for the geometry shown in Figure 5(b), are

$$\text{at } \psi = 0\text{: } \frac{\mathrm{d}\psi}{\mathrm{d}s} = \frac{1}{R_c}, \quad \text{at } \psi = \theta^*\text{: } \frac{\mathrm{d}\psi}{\mathrm{d}s} = 0. \tag{31a, b}$$

Initially, the orientation of the asymptote θ^* is unknown, nevertheless equation (29) can be integrated to give

$$\left(\frac{\mathrm{d}\psi}{\mathrm{d}s}\right)^2 = -2\lambda^2\cos(\theta^* - \psi) + A. \tag{32}$$

The unknowns θ^* and A are found from the boundary conditions. In particular, the peel-off angle becomes

$$\theta^* = \arccos\left[1 - \frac{1}{2(R_c\lambda)^2}\right]. \tag{33}$$

Then the curvature of the web is obtained as

$$\frac{1}{R(s)} = \frac{\mathrm{d}\psi}{\mathrm{d}s} = \lambda[2(1-\cos(\theta^* - \psi))]^{1/2}. \tag{34}$$

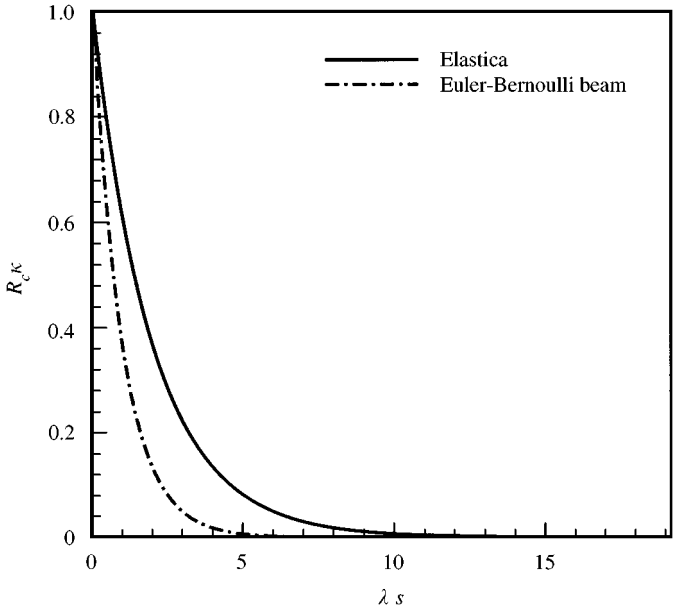

Figure 6. Comparison of the normalized web-curvature $R_c\kappa(s)$ in the bending region for the beam and elastica models along the normalized beam length λs.

Here this equation is integrated numerically. However, it can also be put into the form of an elliptic integral, and be evaluated from standard tables (Frisch–Fay 1962).

2.2.3. *Summary and comments on the web curvature*

The curvature relationships given by equations (27) and (34) are compared in Figure 6. This figure shows that the beam-solution underestimates the curvature variation. Therefore, the pull-down pressure T/R, in the transition region, will be lower with the beam approach. Let the *transition region* be defined as the region where the web-curvature reduces from $1/R_c$ to $0{\cdot}01/R_c$. Then the transition-region length for the beam equation becomes

$$\varepsilon_t = -\frac{1+\ln(100)}{\lambda} + R_c\theta^* = \frac{\ln(100)}{\lambda} \tag{35}$$

For the elastica equation this expression is

$$\varepsilon_t = \frac{1}{\sqrt{2}\lambda}\int_0^{\psi_\varepsilon} \frac{\mathrm{d}\psi}{[1-\cos(\theta^*-\psi)]^{1/2}},$$

where

$$\psi_\varepsilon = \arccos\left[1-\frac{1}{2(R_c\lambda)^2}\right] - \arccos\left[1-\frac{10^{-4}}{2(R_c\lambda)^2}\right]. \tag{36}$$

Figure 6 shows that the transition length is approximately $4{\cdot}6/\lambda$ for the beam solution and $10/\lambda$ for the elastica solution. The peel-off angle θ^* and the transition length are calculated for a few applications of interest (Table 1) and they are presented in Table 2. Here, it can be seen that the beam solution gives good results for the peel-off angle but underestimates ε_t by more than one-half.

TABLE 1

Physical parameters for some webs of practical interest

Material	c (μm)	T (N/m)	E (GPa)	R (m)
Magnetic tape	15	100	4	0·003
PET-film	150	200	4	0·15
Paper	158	70	6.9	0·15

TABLE 2

The peel-off angle and transition-region length for webs given in Table 1

		Beam equation		The elastica	
Material	λ^{-1} (mm)	θ^*	ε_t (mm)	θ^*	ε_t (mm)
Magnetic tape	0·111	2·1235°	0·51	2·1236°	1·66
PET-film	2·486	0·9497°	11·44	0·9497°	27·61
Paper	5·967	2·2792°	27·47	2·2793°	66·27

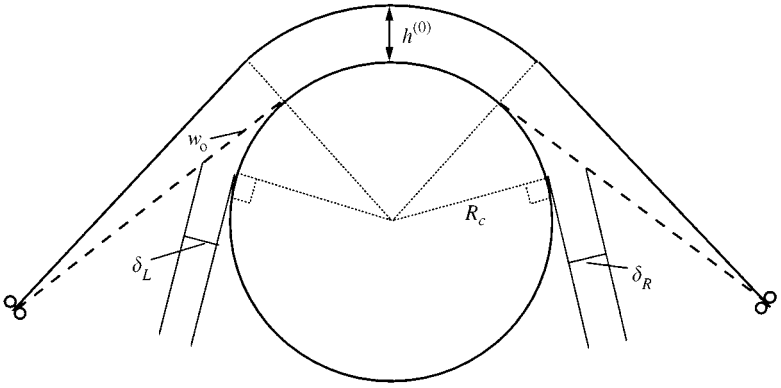

Figure 7. Schematic view of the initial guess for the web-reverser clearance, $h^{(0)}$, and the reverser geometry, δ, in equation (37).

2.3. THE WEB-REVERSER CLEARANCE

The clearance h between the web and the reverser, at a given location (x, y) on the web, is measured along the normal to the surface of the reverser as shown in Figure 7. This is represented mathematically as

$$h(x, y) = w(x, y) + \delta(x),$$

with

$$\delta(x) = \begin{cases} \delta_L(x) & \text{left flat-region,} \\ 0 & \text{wrap-region,} \\ \delta_R(x) & \text{right flat-region,} \end{cases} \tag{37}$$

where $\delta_L(x)$ and $\delta_R(x)$ represent the clearance between the initial reference state of web and the reverser, on the flat region of the web. In the solution method described in Section 4, the function $\delta(x)$ remains constant throughout the solution process.

3. FLUID MECHANICS OF THE AIR-REVERSER

As indicated before the web-reverser clearance h is smaller than the other dimensions of the problem. This allows the flow velocity in the direction normal to the reverser surface w^* to be neglected, and the in-plane flow velocities u^* and v^*, and the air pressure p to be averaged in the normal direction. The hole distribution over the surface of the reverser is averaged locally. For example, using the parameters given in Figure 8 the *hole density* becomes $\alpha = \pi r_h^2/bd$. The governing equations for the steady-state air-flow in the web-reverser clearance then become the modified mass-continuity and Navier–Stokes equations given by Müftü *et al.* (1998b). These equations, expressed in a Cartesian coordinate frame (x^*, y^*) located on the reverser surface as indicated in Figure 1, are

$$\frac{\partial hu^*}{\partial x^*} + \frac{\partial hv^*}{\partial y^*} = \alpha U,$$

$$\rho\left(u^*\frac{\partial u^*}{\partial x^*} + v^*\frac{\partial u^*}{\partial y^*}\right) = -\frac{\partial p}{\partial x^*} + \mu\left(\frac{4}{3}\frac{\partial^2 u^*}{\partial x^{*2}} + \frac{\partial^2 u^*}{\partial y^{*2}} + \frac{1}{3}\frac{\partial^2 v^*}{\partial x^*\partial y^*}\right) - 2\frac{\tau_{z^*x^*}}{h} - \alpha\rho U\frac{u^*}{h},$$

$$\rho\left(u^*\frac{\partial v^*}{\partial x^*} + v^*\frac{\partial v^*}{\partial y^*}\right) = -\frac{\partial p}{\partial y^*} + \mu\left(\frac{\partial^2 v^*}{\partial x^{*2}} + \frac{4}{3}\frac{\partial^2 v^*}{\partial y^{*2}} + \frac{1}{3}\frac{\partial^2 u^*}{\partial x^*\partial y^*}\right) - 2\frac{\tau_{z^*y^*}}{h} - \alpha\rho U\frac{v^*}{h}, \tag{38}$$

where U is the air velocity through the reverser holes as depicted in Figure 8. The web-reverser clearance h is measured along a normal to the reverser surface. The flow is turbulent in the web-reverser clearance as shown by the high value of the Reynolds number $\mathrm{Re} = \rho V h/\mu \approx 5200$. Thus, a reasonable estimate for the shear stresses $\tau_{z^*x^*}$ and $\tau_{z^*y^*}$, which occur at the web and reverser surfaces, can be obtained from the $\frac{1}{7}$th-power-velocity

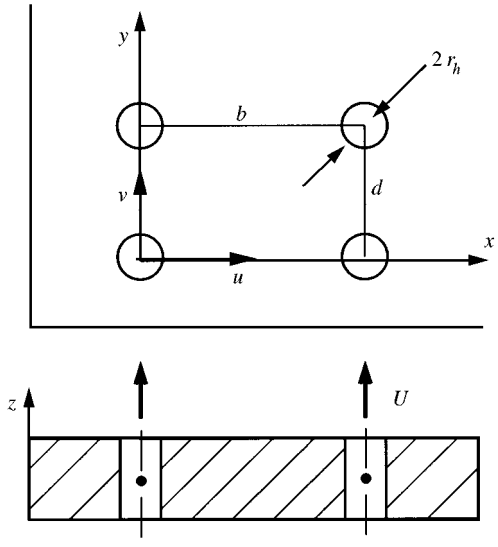

Figure 8. Details of the pressure holes on the surface of the air reverser.

distribution law (Schlicting 1987) for the case of turbulent flow in a two-dimensional channel

$$\tau_{z^*x^*} = \frac{1}{2}\rho 0{\cdot}0676 \cos\theta \left(\frac{\rho h}{\mu}\right)^{\lambda'} (u^{*2} + v^{*2})^{(2-\lambda')/2},$$
$$\tau_{z^*y^*} = \frac{1}{2}\rho 0{\cdot}0676 \sin\theta \left(\frac{\rho h}{\mu}\right)^{\lambda'} (u^{*2} + v^{*2})^{(2-\lambda')/2}, \tag{39}$$

where $\theta = \tan^{-1}(v^*/u^*)$ and $\lambda' = \frac{1}{4}$ (Müftü *et al.* 1998b). The air velocity through the holes U depends on the pressure drop between the supply pressure inside the reverser and the local air pressure in the clearance. This velocity can be expressed by using the Bernoulli's equation across a hole. However, frictional losses at the exit of the hole need to be considered. This is done by using a *discharge coefficient*, $0 \leq \kappa \leq 1$. Thus, the equation representing the air velocity through the holes becomes

$$U = \kappa U_0 (1 - p/p_0)^{1/2}, \tag{40}$$

where $U_0 = \sqrt{2p_0/\rho}$. The effect of the momentum of the incoming air near the holes is only approximately included by this method. However, the overall momentum balance should be preserved if the correct value of κ can be found. Experiments show that for the reversers of interest, κ varies between 0·65 and 0·9 (Müftü *et al.* 1998b).

On the outer periphery of the web-reverser clearance, the air velocity is substantially high. Therefore, the following exit boundary condition for the air pressure is prescribed:

$$p = P_a - \tfrac{1}{2}\rho\kappa_b(u^{*2} + v^{*2}) \tag{41}$$

on the outer boundary, where κ_b is a discharge coefficient for the exit flow at the boundary and $P_a = 0$ is the ambient pressure. A value of $\kappa_b = 1$ was used in this paper. No exit conditions for the flow are necessary.

4. NUMERICAL SOLUTION

4.1. Solution of the Shell Equations

The radial equilibrium equation (15) (called the w-equation heretofore) and the stress function equation (18) (ϕ-equation) are coupled through the radial deflections w and the stress resultants (16). In this work, a staggered solution is used, where the w- and ϕ-equations are solved separately in an iteration loop. Thus, the nonlinear coupling due to the right-hand side of equation (18) is avoided and the array storage requirement of the fully coupled w–ϕ solution is reduced by one half.

The governing equations and the boundary conditions are discretized using second-order accurate, central finite-difference formulas, using M_s nodes in the x- and N_s nodes in the y-direction. The discretization transforms the (x, y) plane to the (i, j) mesh, where a node of the mesh is identified by its node number k, ($k = (i-1)N_s + j : i \in [1, M_s]$ and $j \in [1, N_s]$). A uniform mesh spacing is enforced. A similar discretization for the w-equation is described in detail in Müftü (1994). The w-equation is nonlinear due to w_r and the fluid–structure coupling. The linearization of this equation is described below.

The ϕ-equation is represented in the following matrix form, following a similar spatial discretization:

$${}^{\phi}\mathbf{K}\,\boldsymbol{\phi} = {}^{\phi}\mathbf{r}, \tag{42}$$

where ${}^{\phi}\mathbf{K}$ is a banded matrix, with bandwidth $4N_s + 1$, representing the biharmonic operator, $\boldsymbol{\phi}$ is the vector of stress function values at the mesh points, and ${}^{\phi}\mathbf{r}$ is the vector obtained upon discretization of the right-hand side of equation (18).

4.1.1. *Solution of the w-equation*

Equation (15) is nonlinear and it is solved iteratively with the Newton's method. This method starts the solution with an initial guess $w_k^{(n=0)}$, where n is the iteration number and k a node on the solution mesh. The iterations are updated as

$$w_k^{(n+1)} = w_k^{(n)} + \Delta w_k^{(n+1)}, \tag{43}$$

where $\Delta w_k^{(n+1)} = w_k^{(n+1)} - w_k^{(n)}$. In order to obtain the correction term $\Delta w_k^{(n+1)}$, the discretized residual ${}^{w}r_k$ is linearized around a known iteration step n using a Taylor series expansion

$${}^{w}r_k^{(n+1)} = {}^{w}r_k^{(n)} + \sum_{l=1}^{N_s M_s} \frac{\partial {}^{w}r_k}{\partial w_l}\bigg|^{(n)} \Delta w_l^{(n+1)} + \sum_{l=1}^{N_s M_s} \frac{\partial {}^{w}r_k}{\partial p_l}\bigg|^{(n)} \Delta p_l^{(n+1)} \quad \text{for all } k. \tag{44}$$

The higher-order terms of the expansion are not shown in the above equation. Equation (44) can be expressed in vectorial form as

$${}^{w}\mathbf{K}^{(n)} \boldsymbol{\Delta}\mathbf{w}^{(n+1)} = {}^{w}\mathbf{r}^{(n)} - \mathbf{I}\boldsymbol{\Delta}\mathbf{p}^{(n+1)}, \tag{45}$$

where ${}^{w}\mathbf{K}$ is the tangent stiffness matrix, $\mathbf{I}$ is the identity matrix, $\boldsymbol{\Delta}\mathbf{p}^{(n+1)}$ is the vector containing change in air pressure at the current iteration step, and ${}^{w}\mathbf{r}^{(n)}$ is the residual vector for equation (15). The term $\mathbf{I}\boldsymbol{\Delta}\mathbf{p}^{(n+1)}$ arises from the fluid–structure coupling. The tangent stiffness matrix ${}^{w}\mathbf{K}$ is a function of the web deflection $\mathbf{w}^{(n)}$, and therefore equation (45) is nonlinear. Two nonlinear terms contribute to the tangent stiffness matrix. The first one is due to the reference state and is of the form $-(D\nabla^4 w_r + D_s w_r)$ along the center-line of the web. The second one is due to the fluid–structure coupling and comes from the $\partial p/\partial w$ component of equation (44); this derivative is approximated by

$$\frac{\partial p_k}{\partial w_k} \simeq \left| \frac{p_k^{(n)} - p_k^{(n-1)}}{w_k^{(n)} - w_k^{(n-1)}} \right|. \tag{46}$$

4.2. Solution of the Fluid Equations

The air pressure under the web is obtained from a simultaneous, numerical solution of equations (38a–c). Details of this solution are given by Müftü *et al.* (1997). This method uses pseudo-compressibility where the continuity equation is modified as

$$\frac{\partial ph}{\partial t} + \rho a^2 \left(\frac{\partial hu^*}{\partial x} + \frac{\partial hv^*}{\partial y} \right) = \rho a^2 \alpha U. \tag{47}$$

The parameter a, the artificial speed of sound, and the pseudo-time, t, serve as relaxation parameters in this approach. The momentum equations (38b, c) are augmented by $\rho\partial u^*/\partial t$ and $\rho\partial v^*/\partial t$ on their left-hand sides, respectively. These equations are discretized in space by a second-order accurate central finite difference scheme, and in time by the Crank–Nicholson averaging. The uniform space mesh involves M_f nodes in the x^*-direction and N_f nodes in the y^*-direction. The system of equations is linearized with Newton's method. Use of centered difference formulas introduces aliasing error which is eliminated by using artificial viscosity. The discretized system is represented as

$$-\mathbf{r}^{(n)} - \mathbf{C}_e \mathbf{q}^{(n)} = (\mathbf{J}^{(n)} - \mathbf{C}_i)\boldsymbol{\Delta}\mathbf{q}^{(n+1)}, \tag{48}$$

where $\mathbf{r}^{(n)} = \{{}^{p}\mathbf{r}^{(n)}, {}^{u*}\mathbf{r}^{(n)}, {}^{v*}\mathbf{r}^{(n)}\}^{\mathrm{T}}$, $\mathbf{q}^{(n)} = \{\mathbf{u}^{*(n+1)}, \mathbf{v}^{*(n+1)}, \mathbf{p}^{(n+1)}\}^{\mathrm{T}}$, $\mathbf{J}^{(n)}$ is the Jacobian matrix and the matrices $\mathbf{C}_e$ and $\mathbf{C}_i$ are the artificial viscosity operator matrices. The band-width of the matrix $(\mathbf{J}^{(n)} - \mathbf{C}_i)$ is $6N_f + 7$. The Jocobian matrix in equation (48) is a function of $\mathbf{q}^{(n)}$. Therefore, the matrix $(\mathbf{J}^{(n)} - \mathbf{C}_i)$ is inverted at every iteration step. The successive-over-relaxation method is used to solve equation (48).

4.3. Coupled Solution of the Fluid and the Shell Equations

The fluid and the shell equations are solved on different meshes. The fluid mesh and the solid mesh are not required to have one-to-one correspondence. Nine-point biquadratic interpolation formulas are used to convey the information between the meshes. The interpolation formulas are given in Cook *et al.* (1989, pp. 176–180). The following algorithm is used to obtain the coupled solution:

(i) set $\mathbf{w}^{(0)}, \mathbf{h}^{(0)}, \phi^{(0)}, n = 1$, calculate ${}^{w}\mathbf{r}^{(0)}$; repeat until $L_2({}^{w}\mathbf{r}^{(n+1)}) < \varepsilon L_2({}^{w}\mathbf{r}^{(0)})$ or $n >$ Iter-$\mathrm{Lim}_{\mathrm{web}}$;
(ii) interpolate from shell mesh to fluid mesh;
(iii) $n_a = 1$; repeat until $L_2(\mathbf{r}^{(n_a+1)}) < \varepsilon$ or $n_a >$ $\mathrm{IterLim}_{\mathrm{air}}$;
(iv) solve equation (48);
(v) $\mathbf{q}^{(n_a+1)} = \mathbf{q}^{(n_a)} + \Delta\mathbf{q}^{(n_a+1)}$;
(vi) calculate $L_2(\mathbf{r}^{(n_a+1)})$;
(vii) set $n_a = n_a + 1$;
(viii) interpolate from fluid mesh to shell mesh;
(ix) calculate ${}^{w}\mathbf{K}^{(n)}$ and ${}^{w}\mathbf{r}$;
(x) solve the w-equation (45);
(xi) $\mathbf{w}^{(n+1)} = \mathbf{w}^{(n)} + \Delta\mathbf{w}^{(n+1)}$;
(xii) solve the ϕ-equation (42);
(xiii) calculate $L_2({}^{w}\mathbf{r}^{(n+1)})$;
(xiv) set $n = n + 1$.

5. RESULTS

In this section, the steady-state solutions of three generic cases are presented. The geometry and the hole distribution of these cases are given in Tables 3 and 4. In Cases 1 and 3, the reverser has holes only on the left and right sides of the reverser, and no holes exist on the lateral edges of the middle section. The hole densities are $\alpha = 0{\cdot}025$ and $0{\cdot}05$ for these cases. On the other hand, in Case 2, the hole density $\alpha = 0{\cdot}025$ is distributed uniformly around the outer periphery of the reverser area. Using this reverser, a 200 μm thick, 1·016 m wide and 1·016 m long web is modeled under various operating conditions. In particular, the effects of initial web-reverser clearance $h^{(0)}$, supply pressure p_0, and hole density distribution α are considered.

5.1. The Steady-State Equilibrium

The steady-state web deflections, air pressure and velocity distributions of Cases 1–3 are shown in Figures 9–11, respectively. These plots represent typical solutions of the coupled problem. The common parameters of these cases are $p_0 = 500$ Pa and $T = 120$ N/m.

These figures show that maximum air pressure is located along the web center-line, $y = L_y/2$, and that the air pressure gradually drops toward the edges. On the left and right edges, air exits the reverser area in a fairly uniform manner. On the periphery, the air pressure becomes subambient due to the pressure boundary condition (41). In Cases 1 and 3,

where the lateral edges of the reverser have no holes, there is a large air pressure variation in the transverse direction and the air-flow is distinctly two-dimensional. More air leaves the web-reverser clearance from these edges. In contrast to this situation, in Case 2, where the lateral edges of the reverser contain pressure holes, the air-flow from the lateral edges is more uniform and the air velocity is reduced. In this case, the overall air pressure in the clearance is higher, partly due to reduced side flow, and partly due to increased volume of air injected into the clearance. The effect of using side holes on increasing the air pressure in the web- reverser clearance has been discussed by Müftü *et al.* (1998a).

The web deflection w shown in Figures 9–11 is measured with respect to the *initial reference state*, w_o. These figures show that in the transverse direction, the nonwrapped region of the web undergoes a relative deflection at its edges as compared to its middle region. In contrast, the wrapped region remains relatively flat. This difference in deflection behavior is due to the additional in-plane stiffness, D_s, shown by equation (15), that the web gains in the wrap- region.

The onset of web contact with the reverser

The ultimate goal of using a reverser in the web path is to provide a mechanism for the web to change its direction without contact. The mechanics of the onset of contact can be explained by studying the hole-density distributions presented in Cases 1–3. Figure 12 shows the cross sections of the web deflection and air pressure along the web center-line $(x, L_y/2)$.

For the hole density of Cases 1 and 2, where $\alpha = 0{\cdot}025$, the web floats closer to the reverser, in the nonwrapped area, compared to Case 3, as shown in Figure 12(a). This is due to insufficient air pressure p under the flat region of the web, which is expected to

TABLE 3

The reverser-geometry parameters

R_c	0·25 m
$\bar{y}_C$	0·115 m
$h^{(0)}$	0·003 m
$(\bar{x}_A, \bar{y}_A)$	(−0·26,0) m
$(\bar{x}_E, \bar{y}_E)$	(0·26,0) m

TABLE 4

The hole-density distribution of Cases 1–3

Hole density case No.	x-range (m)			y-range (m)			α
1	0·0	–	0·3	0·0	–	1·016	0·025
	0·3	–	0·716	0·0	–	1·016	0·0
	0·716	–	1·016	0·0	–	1·016	0·025
2	0·0	–	0·3	0·0	–	1·016	0·025
	0·3	–	0·716	0·0	–	0·1406	0·025
	0·3	–	0·716	0·1406	–	0·8755	0·0
	0·3	–	0·716	0·8755	–	1·016	0·025
	0·716	–	1·016	0·0	–	1·016	0·025
3	0·0	–	0·3	0·0	–	1·016	0·05
	0·3	–	0·716	0·0	–	1·016	0·0
	0·716	–	1·016	0·0	–	1·016	0·05

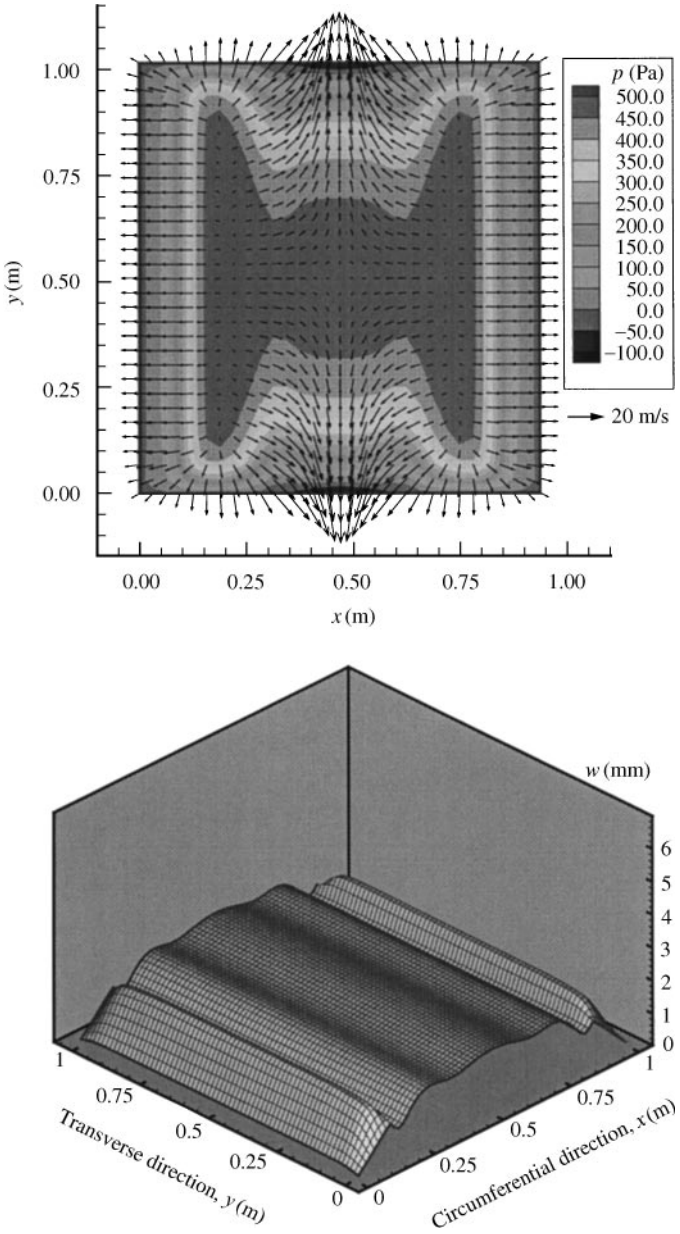

Figure 9. The calculated air pressure p, air-flow vectors, web deflection w for hole distribution Case 1, for $p_0 = 500$ Pa and $T = 120$ N/m.

balance the pull-down pressure T/R. The localized deficiency of p with respect to T/R can be seen in Figure 12(b). Note that there is no contact between the web and the reverser in these two cases, and the whole system is in equilibrium. However, the lowest web-reverser separation is $h_{\min} \simeq 1$ mm, at $x = 0{\cdot}16$ and $0{\cdot}84$ m locations, whereas at the center the separation is $h_{\text{mid}} \simeq 1{\cdot}9$ mm for Case 1 and $h_{\text{mid}} \simeq 3{\cdot}7$ mm for Case 2. The nonuniform and narrow web-reverser separation achieved for Cases 1 and 2 makes the web susceptible to contact.

On the other hand, in Case 3, where the hole density under the flat region of the web is increased to $\alpha = 0{\cdot}05$, the air pressure becomes higher, as shown in Figure 12(b). Thus, the

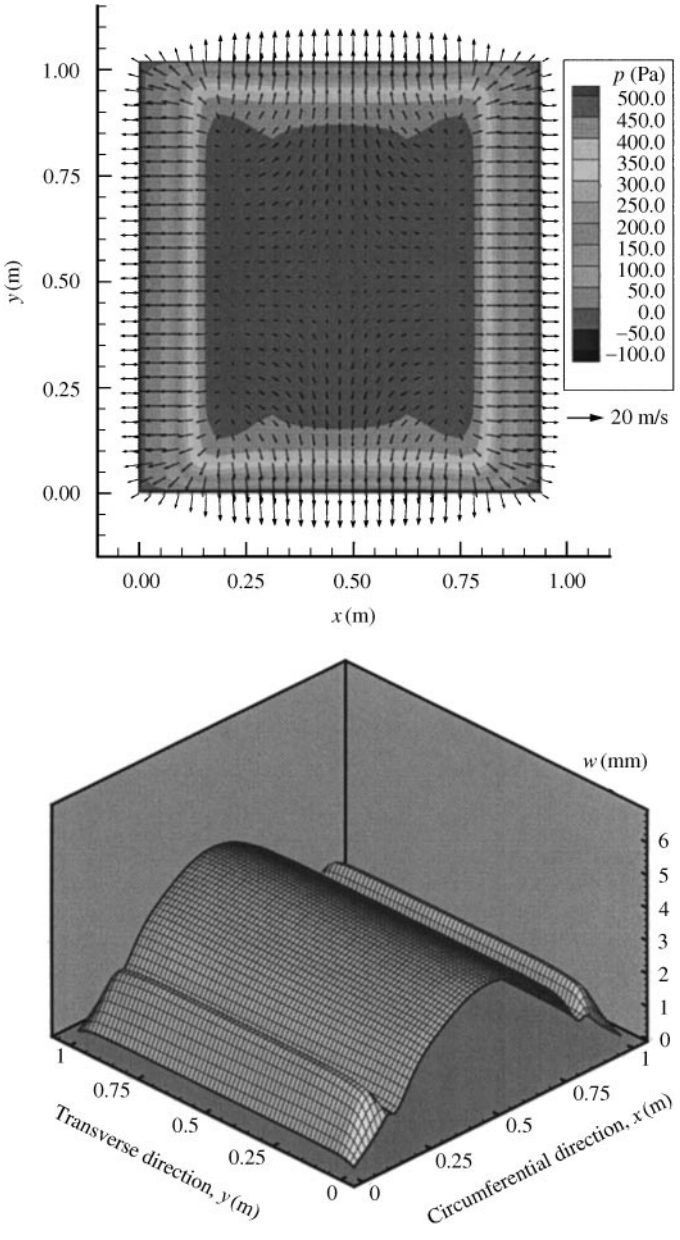

Figure 10. The calculated air pressure p, air-flow vectors, web deflection w for hole distribution Case 2, for $p_0 = 500$ Pa and $T = 120$ N/m.

web deflects away from the reverser surface, as depicted in Figure 12(a), and the susceptibility to contact is reduced.

5.2. Effect of Initial Web-Reverser Separation

The iterative method used to solve the governing equations requires an initial guess for the distribution of the web-reverser clearance $h^{(0)}$. This initial value is depicted schematically in

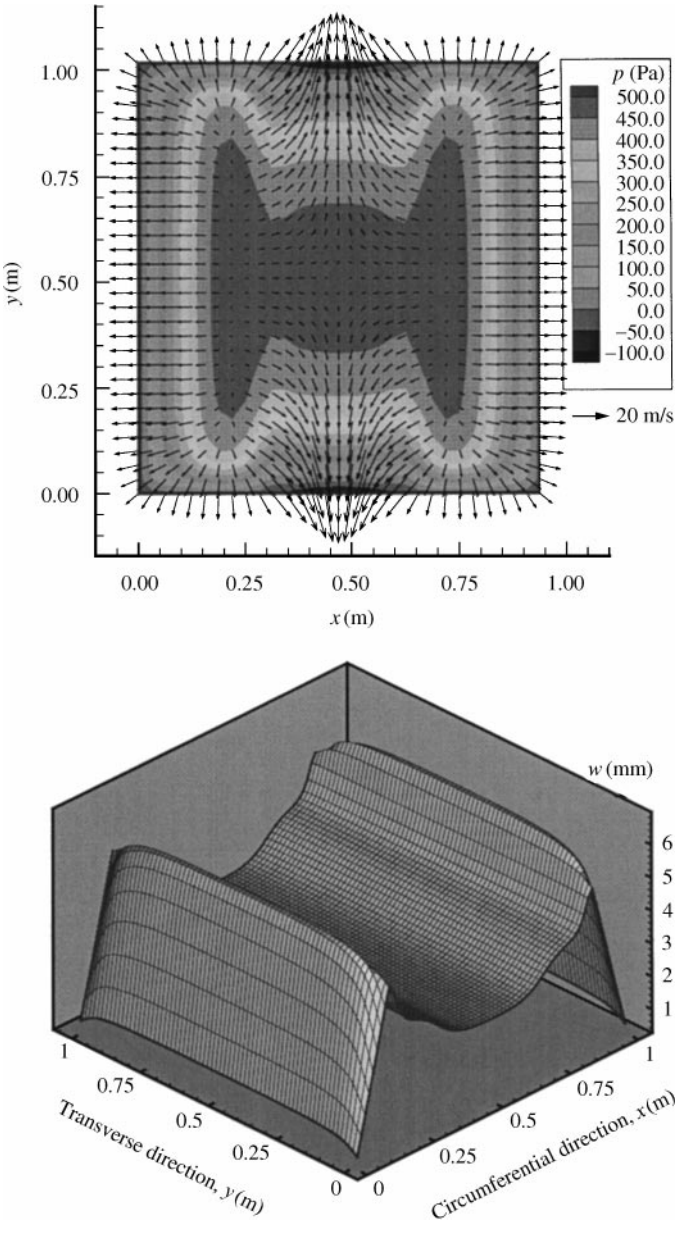

Figure 11. The calculated air pressure p, air-flow vectors, web deflection w for hole distribution Case 3 for $p_0 = 500$ Pa and $T = 120$ N/m.

Figure 7. The effect of starting the solution process with different initial clearance values was tested for $h^{(0)} = 1, 2$ and 3 mm. This test was done for the tension, $T = 120$ N/m, and supply pressure, $p_0 = 500, 750, 1000, 1250, 1500$ Pa. Table 5 gives the web-reverser clearance at the mid-point of the web, $h_{\text{mid}} = h(L_x/2, L_y/2)$, as a function of $h^{(0)}$ and p_o. This table shows that starting the model at different $h^{(0)}$ values results in the same h_{mid} values. Thus, it is concluded that the steady-state solution of the problem is independent of the initial guess of the web- reverser clearance.

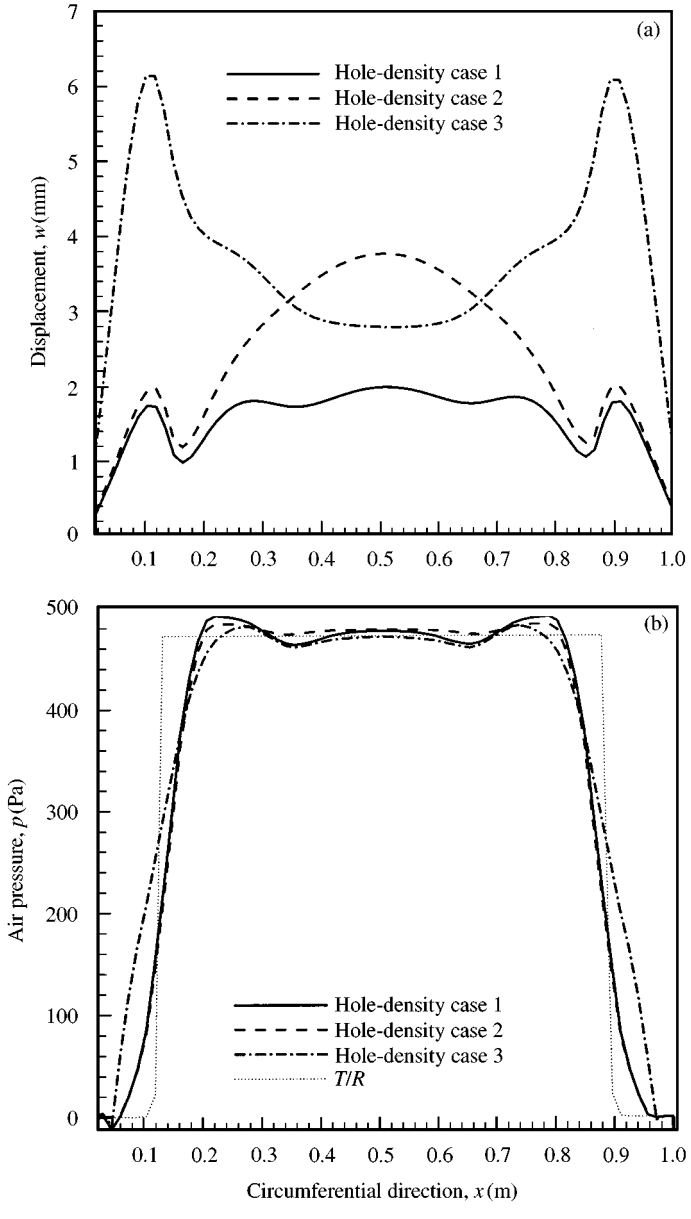

Figure 12. Cross-section of the results for hole density Cases 1–3, at $y = L_y/2$. (a) The web deflection w with respect to the *initial reference state* w_o. (b) The air pressure p and pull-down pressure T/R.

5.3. Effect of Web Tension and Supply Pressure

In order to investigate the effect of the supply pressure p_0 on the steady state of the web-reverser clearance, p_0 was varied between 500 and 700 Pa with 20 Pa increments. The results are given in Figure 13. The mid-cross sections of the web-reverser clearance $h(x, L_y/2)$ and the air pressure $p(x, L_y/2)$ are plotted for different p_0 values in Figure 13(a). The mid-point and minimum web-reverser clearance values h_{mid} and h_{min}, and the total

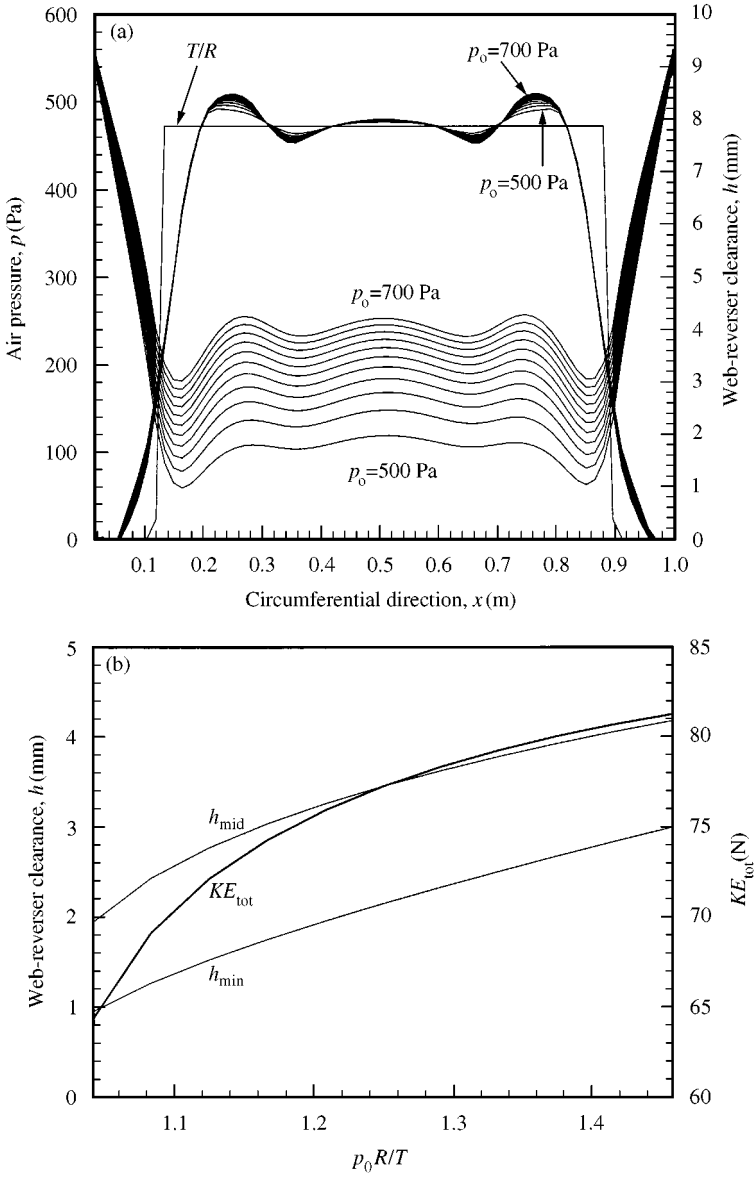

Figure 13. (a) The web deflection w and air pressure p, along the web center-line $y = L_y/2$, as a function supply pressure p_0, with 20 Pa increments. (b) The mid-point and minimum web-reverser clearance h_{mid} and h_{min}, and the total kinetic energy of air, as a function of the nondimensionalized supply pressure p_0R/T. Both figures represent Case 1 with $T = 120$ N/m, $R = 0{\cdot}25$ m.

kinetic energy in the clearance, $KE_{tot} = \int_A \frac{1}{2}\rho|\mathbf{v}|^2\,\mathrm{d}A$, where $\mathbf{v}$ is the air velocity vector, and A the surface area of the web, are plotted in Figure 13(b).

Figure 13(a) shows that the air-pressure distribution remains nearly constant, at a value close to the pull-down pressure, even though more air is injected into the clearance at higher supply pressures. On the other hand, the web-reverser clearance h increases considerably at higher p_0 values. This clearance increase, in fact, prevents more pressure built- up to occur. Based on these results, it is concluded that the pull-down pressure has the maximum

TABLE 5

The steady-state values of the mid-point web-reverser clearance h_{mid} obtained with three different initial clearance values $h^{(0)}$ for α of Case 1

Supply pressure, p_o (Pa)	$h_{mid} = h(L_x/2, L_y/2)$ (cm)		
	For $h^{(0)} = 1$ mm	For $h^{(0)} = 2$ mm	For $h^{(0)} = 3$ mm
500	1·9416	1·9416	1·9417
750	4·4584	4·4584	4·4584
1000	5·4818	5·4818	5·4818
1250	6·2496	6·2496	6·2496
1500	6·9409	6·9409	6·9409

influence on the steady-state equilibrium of the system. Figure 13(b) shows that the excess energy of incoming air, at higher supply pressures, is spent on increasing the overall velocity in the clearance.

6. SUMMARY AND CONCLUSIONS

A relatively simple mathematical model for the steady-state fluid–structure interaction between a web and the air-cushion generated by an air-reverser is presented. The web is modeled as a thin, flexible cylindrical shell whose strain-free reference state is self-adjusting according to the interaction between the air-cushion and pull-down pressures. The airflow in the web-reverser clearance is modeled by a two-dimensional, averaged form of the momentum and mass balance equations with nonlinear source terms. The coupled system equations are solved numerically. It is shown that, at steady state, the air-cushion pressure in the clearance is nearly equal to the pull-down pressure. The equilibrium is established so that increasing the supply pressure causes the web to deflect away from the reverser surface, thus creating a wider web-reverser separation and keeping the average clearance air pressure nearly constant. While the web may be in overall equilibrium with the air-cushion pressure, near the entry and exit sides of the reverser, the air pressure may not be sufficient to counteract the pull-down pressure. When this occurs the web floats closer to the reverser, and in these areas contact may occur. Increasing the hole density in the entry and exit sides helps enough air pressure to be generated to counteract the pull-down pressure.

ACKNOWLEDGEMENTS

This work was primarily supported by Eastman Kodak Company. Parts of this work were also supported by grants from Hewlett Packard Laboratories and NSF grant ECS-9615027. The first author gratefully acknowledges this support. The authors also wish to thank Drs Timothy Lewis and Alan Brewen from Eastman Kodak Company, Richard Benson from Pennsylvania State University and Alan Rogers from M.I.T. for helpful discussions throughout the course of this work.

REFERENCES

BARLOW, E. J. 1967 Derivation of governing equations for self acting foil bearing. *ASME Journal of Lubrication Technology* **89,** 334–340.

BATHE, K.-J. 1996 *Finite Element Procedures*. New Jersey: Prentice-Hall.
BENSON, R. C. & D'ERRICO, J. R. 1991 The deflection of an elastic web wrapped around a surface of revolution. *Mechanics of Structures & Machines* **19,** 467–486.
BENSON, R. C. 1993 The interfacial mechanics of a tape wrapped around a flexible bumpy roll. *Tribology Transactions* **36,** 375–380.
BENSON, R. C. 1998 Stiff elastic tape wrapped onto a drum. *Journal of Applied Mechanics* **65,** 870–874.
COOK, R. D., MALKUS, D. S. & PLESHA, M. E. 1989 *Concepts and Applications of Finite Element Analysis*. New York: Wiley.
DONNELL, L. H. 1976 *Beams, Plates and Shells*. New York: McGraw-Hill.
ESHEL, A. 1979 Numerical solution of the planar hydrostatic foil bearing. *ASME Journal of Lubrication Technology* **101,** 86–91.
FRISCH-FAY, R. 1962 *Flexible Bars*. London: Butterworths.
FUNG, Y. C. & WITTRICK, W. H. 1955 A boundary layer phenomenon in the large deflexion of thin plates. *Quarterly Journal of Mechanics and Applied Mathematics* **8,** 191–210.
GROSS, W. A. (ed.) 1980 *Fluid Film Lubrication*. New York: Wiley.
LIN, C. C. & MOTE, JR., C. D. 1995 Equilibrium displacement and stress distribution in a two-dimensional, axially moving web under transverse loading. *Journal of Applied Mechanics* **62,** 772–779.
LIN, C. C. & MOTE, JR., C. D. 1996 The wrinkling of thin, flat, rectangular webs. *Journal of Applied Mechanics* **63,** 774–779.
MÜFTÜ, S. 1994 The Transient Foil Bearing Problem in Magnetic Recording. Ph.D. Dissertation, Department of Mechanical Engineering, University of Rochester, Rochester, NY, U.S.A.
MÜFTÜ, S. & BENSON, R. C. 1995 A study of cross-width variations in the two dimensional foil bearing problem. *ASME Journal of Tribology* **118,** 407–414.
MÜFTÜ, S., LEWIS, T. S. & COLE, K. A. 1997 A numerical solution of the Euler's equations with nonlinear source terms in modelling the fluid dynamics of an air reverser. *Proceedings of Information Storage and Processing Systems Symposium*, ASME-IMECE, Dallas, TX, ISPS-3, pp. 39–48.
MÜFTÜ, S., LEWIS, T. S., COLE, K. A. & BENSON, R. C. 1998a Modelling of fluid dynamics of air reversers. *Journal of Applied Mechanics* **65,** 171–177.
MÜFTÜ, S., LEWIS, T. S., CZUPRYNSKI, D. M. & COLE, K. A. 1998b A simple two dimensional model for incompressible, viscous fluid flow in an externally pressurized narrow channel. Internal report, M.I.T. Haystack Observatory, Westford, MA.
ONO, K. & EBIHARA, T. 1984 Improved Green's function in tape deflection and solutions of head contour with uniform contact pressure. *Tribology and Mechanics of Magnetic Recording Systems, Society of Tribologists and Lubrication Engineers*, Special Publication SP-16, pp. 97–102.
PIMENOV, V. G. & GALIMOV, M. M. 1994 Use of air blankets for the drying and transport of film materials. *Chemical and Petroleum Engineering* **30,** 486–488 (*Translated from Khimicheskoe i Neftyanoe Mashinostronie, No.* 10, 18-20, *Oct.* 1994.)
QUADRACCI, H. R. & MODI, V. 1994 Heat transfer of an inclined Coanda jet to a flexible web. ASME Paper 94-WA/HT-21.
RONGEN, P. M. J. 1990 On numerical solutions of the instationary 2D foil bearing problem. *Tribology and Mechanics of Magnetic Recording Systems, Society of Tribologists and Lubrication Engineers*, Special Publication SP-29, pp. 130–138.
RONGEN, P. M. J. 1994 Finite Element Analysis of the Tape Scanner Interface in Helical Scan Recording. Ph.D. Dissertation, Technical University of Eindhoven, The Netherlands.
SCHLICTING, H. 1987 *Boundary-Layer Theory*. New York: McGraw-Hill.
SUNDARAM, R. & BENSON, R. C. 1989 A Green's function with improved convergence for cylindrically wrapped tapes. *Tribology and Mechanics of Magnetic Recording Systems, Society of Tribologists and Lubrication Engineers*, Special Publication SP-16, pp. 98–110.
TIMOSHENKO, S. P. & WOINKOWSKY-KRIEGER, S. 1987 *Theory of Plates and Shells*. New York: McGraw-Hill.
WILDMANN, M. 1969 Foil bearings. *ASME Journal of Lubrication Technology* **91,** 37–44.

APPENDIX: NOMENCLATURE

C	in-plane stiffness, $Ec/(1-\nu^2)$
C'	$C(1-\nu)/2$
D	bending stiffness, $Ec^3/12(1-\nu^2)$

D_s	shell stiffness
D'	$D(1-\nu)$
E	Young's modulus
H	Heaviside step function
L	typical web length
L_1, L_2	tangency points of a membrane
L_x, L_y	total length and width of the web
M_x, M_y, M_{xy}	bending moment resultants of the web
N_x, N_y, N_{xy}	in-plane stress resultants of the web
N'_x, N'_y, N'_{xy}	in-plane stress resultants of the web at steady state
Q_x, Q_y	normal shear force resultants of the web
P_a	ambient air pressure
R_o	radius variation at the initial reference state
R_c	radius of the air reverser
R, $R(x)$	radius, radius of the web
Re	Reynolds number, $\rho Uh/\mu$
Re^*	modified Reynolds number, $\rho Uh^2/L\mu$
T	external tension
U	air velocity at the exit of an air hole
V	typical air velocity
c	web thickness
h	web-reverser clearance
$h^{(0)}$	initial web-reverser clearance
u^*, v^*, w^*	air velocity components
u, v, w	web deflection components
x^*, y^*, z^*	coordinates for fluid mechanics
x, y, z	coordinates for web mechanics
w	web deflection with respect to w_0
w_0	initial reference state of the web
w_r	self-adjusting reference state of the web
$\bar{w}$	$w - w_r$
p	air pressure
s	longitudinal coordinate for the beam-solution
t	pseudo-time used by the artificial compressibility method
α	air hole distribution density
ε_x, ε_y, ε_{xy}	in-plane strains in the web
ε_t	distance along the unwrapped web where curvature becomes $0{\cdot}01/R_c$
κ_x, κ_y, κ_{xy}	curvatures of the deformed web
κ	discharge coefficient at the hole exit
κ_b	discharge coefficient at the outer periphery of the web
λ	$(T/D)^{1/2}$
μ	viscosity of air
ν	Poisson's ratio
ϕ	the Airy stress function
ψ	angle between the web tangent and the $\bar{x}$ axis in Figure 5(b)
ρ	density of air
$\tau_{z^*x^*}$, $\tau_{z^*y^*}$	shear stress components between air and walls
θ^*	peel-off angle
∇^4	the biharmonic operator

Vector and matrix Operators

$\mathbf{C}_e$	explicit artifical viscosity operator matrix
$\mathbf{C}_i$	implicit artifical viscosity operator matrix
$\mathbf{\Delta p}$	fluid pressure difference between iterations
$\mathbf{\Delta q}$	correction vector of fluid unknowns
$\mathbf{\Delta w}$	correction vector for the w equation
$\boldsymbol{\phi}$	vector of ϕ values on the mesh
$\mathbf{I}$	identity matrix
$\mathbf{J}$	Jacobian matrix of the fluid equation

${}^{\phi}\mathbf{K}$	stiffness matrix of the ϕ equation
${}^{w}\mathbf{K}$	stiffness matrix of the w equation
$\mathbf{q}$	vector of fluid unknowns
${}^{\phi}\mathbf{r}$	residual of the ϕ equation
$\mathbf{r}$	residual of the fluid equation
${}^{w}\mathbf{r}$	residual of the w equation
${}^{p}\mathbf{r}$, ${}^{u^*}\mathbf{r}$, ${}^{v^*}\mathbf{r}$	residual vectors for equations (38a–c)
$\mathbf{u}^*$, $\mathbf{v}^*$, $\mathbf{p}$	vectors of fluid velocity and pressure